Korean J. Chem. Eng., 35(7), 1525-1531 (2018)
DOI: 10.1007/s11814-018-0060-6

pISSN: 0256-1115
eISSN: 1975-7220

Effect of sulfur annealing on the morphological, structural, optical and electrical properties of iron pyrite thin films formed from FeS_2 nano-powder

Thanh Kieu Trinh*,‡, Nguyen Tam Nguyen Truong,‡, Viet Thanh Hau Pham***,‡, Hyoeun Kim**, and Chinho Park**,†**

*Department of Biological Technology and Environment, Yersin University of Da Lat, Lam Dong, Vietnam
**School of Chemical Engineering, Yeungnam University, 280 Daehak-ro, Gyeongsan 38541, Korea
***Deparment of Chemistry, University of Dalat, Lam Dong, Vietnam
(*Received 4 December 2017 • accepted 5 April 2018*)

Abstract−Iron pyrite (FeS_2) thin films were fabricated by spin coating the solution of FeS_2 nanocrystals of ~40 nm in size on glass substrates, followed by annealing in a sulfur environment at different temperatures. The effect of sulfurization temperature on the morphology, structural, optical and electrical properties was investigated. With increase of the sulfurization temperature, the grain size and crystallinity of the films was improved, although some cracks and voids were observed on the surface of thin films. The band gap of the FeS_2 films was decreased at higher sulfurization temperature. The electrical properties were also changed, including the increasing in resistivity and the decrease in Hall mobility, with increase of sulfurization temperature. The change in the optical and electrical properties of the FeS_2 thin films was explained based on the changes of phase, morphology, surface, and grain boundary property.

Keywords: Thin Film, Sulfurization, Morphology, FeS_2 Nano-powder, Spin Coating

INTRODUCTION

Owing to its suitable band gap (0.95 eV) and high optical absorption coefficient in the mid-infrared range (~10^5 cm^{-1}, two magnitudes higher than that of Si) as well as the abundance of the non-toxic source of Fe and sulfur, pyrite (or fool's gold) has been considered as a potential material for low-cost environmental-friendly solar cells and photonic devices of the future [1-3]. Although FeS_2 can be a promising solution for photovoltaics (PVs), actual results have been unsatisfactory. Pyrite FeS_2 devices suffer from a low open-circuit voltage (<200 mV) and an efficiency of ~0% despite the efforts to utilize FeS_2 as an absorber in many kinds of solar cells [4]. Many studies have tried to solve the issue of low open-circuit voltage and lack of efficiency. A sulfur deficiency is one of the main reasons for the low open-circuit voltage and is present as impurity phases in the pyrite bulk, including pyrrhotite, marcasite, and amorphous iron sulfide phases. Sulfur vacancy formation in FeS_2 crystallites has been proposed to induce an energy level within the band gap and cause surface Fermi level pinning, lowering the band gap of FeS_2. In addition, pyrite shows rather complex behavior, including the change in optical and electrical properties in an intriguing way with the change of crystal structure due to a sulfur deficiency [5]. Under this assumption, the sulfurization process may be an effective tool to modify the bandgap of FeS_2. Sulfurization can help compensate for the sulfur deficiency, and improve the properties of FeS_2 for the applications in photovoltaics [6].

Many efforts have been examined to improve the properties of FeS_2 thin films using sulfurization treatment. The properties of FeS_2 thin films were investigated based on natural or synthetic FeS_2 nanocrystals. The Ferrer group was the first group to fabricate FeS_2 thin films by flash evaporation of natural iron pyrite nanocrystals with different thicknesses followed by annealing them in a sulfur atmosphere [7]. The changes in the optical properties produced by thermal annealing of the as-evaporated films in a sulfur atmosphere depend on the thickness of thin films. The absorption edge of the n-type films increases with increase of annealing temperature. However, the photoresponse representative of the intrinsic band gap has not been observed [7]. Besides that, iron pyrite thin films have been synthesized by a variety of solution methods, such as spray pyrolysis [8], electrodeposition [9], chemical bath deposition [10], and sol-gel method [11,12]. The principle of these methods is depositing a film of iron, iron oxide or iron sulfide and annealing the films in sulfur gas environment at different temperatures. These methods provide a pure phase, polycrystalline iron pyrite thin films, which are of p-type conductivity with low resistivity and low mobility. They exhibit no photoelectrochemical response [12]. On the other hand, the features of FeS_2 thin films, including structure, morphology, optical property, composition, and electrical properties (resistivity, Hall mobility, carrier density) are dependent on the experimental procedure used to prepare the films and thermal treatment conditions. Recently, pyrite films have been fabricated by FeS_2 solution deposition. Pyrite nanocrystals were first synthesized by a wet chemical route, such as hot injection [13] or hydrothermal method [14]. The thin films were then formed by spin coating [15] the as-synthesized iron pyrite solution. After the thin films are formed, the sulfurization process is performed to increase the grain size, film density, and carrier diffusion length. However, the structure, mor-

†To whom correspondence should be addressed.
E-mail: chpark@ynu.ac.kr
‡These three authors equally contributed to this work.

phology, optical and electrical properties of these films have not been reported in detail. Because of the complexity and non-uniformity of properties of FeS_2, iron pyrite thin films are still an exciting research objective.

In this study, pyrite (FeS_2) thin films were fabricated by spin coating the solution of FeS_2 nanocrystals of ~40 nm in size, on pure glass substrates, followed by annealing in a sulfur environment. The sulfur annealing procedure was performed at different temperatures to examine the effects of temperature on the structure, morphology, as well as the optical and electrical properties of the films. The changes in stoichiometry, crystallinity, microstructure, and grain size of the films were also investigated in detail.

EXPERIMENT DETAILS

1. Chemicals

Iron (II) chloride tetrahydrate ($FeCl_2{\cdot}4H_2O$, 99%), octadecylamine (ODA, 90%), sulfur element (S, 98%), oleylamine (OLA, 70%), and trioctylamine (TOA, 90%) were purchased from Sigma-Aldrich. The other solvents, including chloroform (CF) and methanol, were commercially available analytical-grade products that were also purchased from Sigma-Aldrich. All chemicals involved in these experiments were used as received.

2. FeS_2 NCs Synthesis

The FeS_2 NCs were synthesized using a hot injection method. In a typical procedure for the preparation of FeS_2 NCs, a mixture of 1.5 mmol $FeCl_2{\cdot}4H_2O$, 10 g ODA, and 10 ml TOA was stirred in a three-necked flask at 150 °C under vacuum for 1 h to form the Fe-surfactant precursor species. In parallel, the sulfur (S) precursor was prepared by adding 9 mmol of elemental sulfur into 5 ml OLA. The mixture was stirred vigorously in air at 70 °C, until the sulfur had been dissolved completely. Subsequently, the S-precursor was injected rapidly into the solution of the Fe-surfactant precursor. The solution was then heated to 220 °C and kept being stirred at this temperature for 2 h under a nitrogen atmosphere to complete the growth of the iron pyrite NCs. The solution was cooled to 100 °C in a water bath and 20 ml chloroform was then added. The iron pyrite NCs were purified by mixed solvent precipitation using chloroform and methanol in a centrifuge at 4,500 rpm for 10 min.

3. FeS_2 Thin Film Fabrication

The FeS_2 solution was prepared using 150 mg FeS_2 in 2 ml of CF. A thin layer of FeS_2 NCs (700 nm) was deposited on top of clean glass at 1,500 rpm for 40 s. The FeS_2 thin films then were annealed by placing the substrate at downstream of the sulfur vapor and nitrogen flow. Sulfurization was performed at different temperatures (250-650 °C) for 1 h. After the sulfurization treatment, the samples were cooled naturally in a N_2 atmosphere.

4. Characterization

The crystal structure of the FeS_2 thin films was examined by X-ray diffraction (XRD, PANalytical, X'Pert-PRO MPD) using Cu Kα radiation and Raman spectroscopy using a WiTec confocal Raman spectrometer (Ar^+ laser, λ=532 nm) at a spectral resolution of 5 cm^{-1}. The surface morphology of the FeS_2 thin films was observed by field emission scanning electron microscopy (FESEM). The chemical composition at the surface of the thin films was examined by X-ray photoelectron spectroscopy (XPS, Thermo Scientific, K-Alpha) using Al Kα monochromatized radiation. The optical properties of the as-synthesized FeS_2 NCs were examined by ultraviolet-visible-near-infrared (UV-Vis-NIR) spectrophotometry (Cary 5000, Varian) from 300 nm to 2,000 nm. The electrical properties were determined by a Hall effect measurement system using the Van der Pauw method.

RESULTS AND DISCUSSION

1. Structural Properties

Fig. 1(a) shows the XRD patterns of iron pyrite films as-deposited and annealed in different sulfurization temperatures. The XRD patterns suggested that increasing the sulfurization temperature leads to an improvement in the crystallinity of the films. The (111), (200), (210), (211), (220), and (311) diffraction peaks were observed from the sulfurized FeS_2 thin films [11]. The crystal growth took place equally in all orientations of FeS_2, which was confirmed by the increased intensity and sharpness for all the peaks mentioned above. The increasing intensity and sharpness of all the peaks indicated that the crystallinity of the films was improved, and the

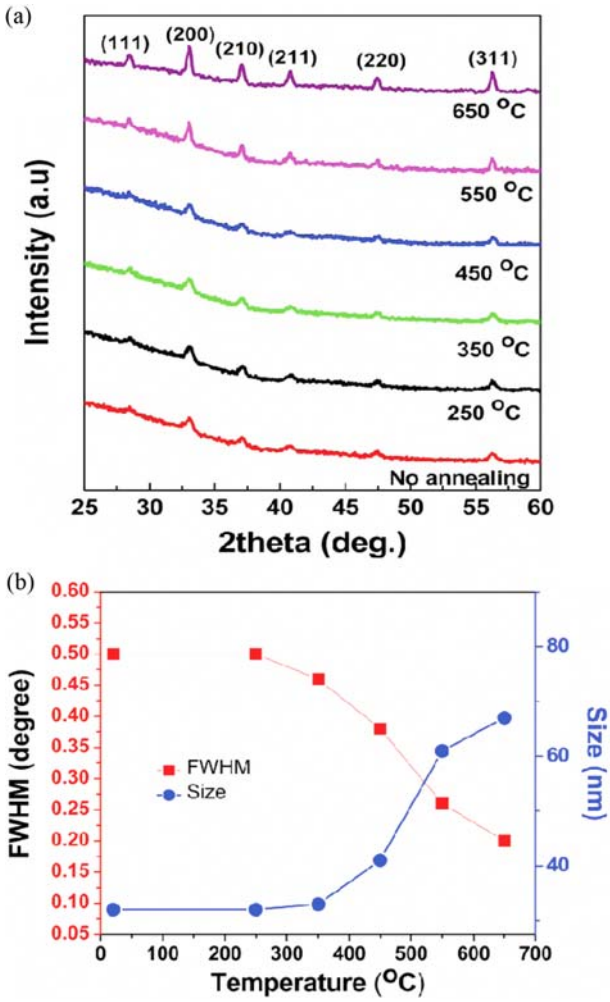

Fig. 1. (a) XRD pattern and (b) grain size of FeS_2 thin films at different sulfurization temperatures.

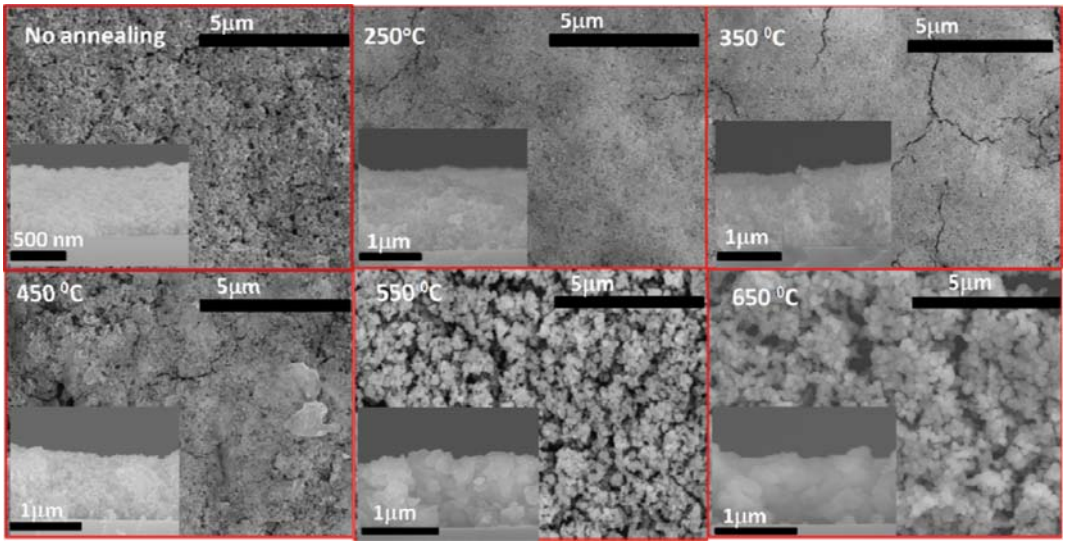

Fig. 2. SEM morphologies of the FeS_2 thin films sulfurized at different temperatures (The inset pictures are cross-section SEM images).

grain size became larger at higher sulfurization temperatures. Fig. 1(b) shows the grains and full width at half maximum intensity (FWHM) of the (200) XRD peaks of the FeS_2 thin films sulfurized at different temperatures, supporting the XRD patterns. The grain size of the formed thin films was determined by FWHM of the (200) XRD peaks by applying the Scherrer's equation with a calculation error of ~10% [16]:

$$D = 0.9\frac{\lambda}{\beta \cdot \cos\theta}$$

where, D is the grain size, λ is the wavelength of X-ray (1.54178 Å), β is the broadening of the diffraction line measured at FWHM in radians, and θ is the diffraction angle.

The grain size of the FeS_2 films was increased with increasing the sulfurizing temperature, as indicated by the decrease of the FWHM values. The grains grew rapidly as temperature was increased in the range of 450 to 550 °C. SEM measurement was used to investigate the effect of the sulfurizing temperature on the grain size and surface morphology of the FeS_2 films. Fig. 2 shows the morphology of the FeS_2 thin films at different sulfurization temperatures. SEM images showed that the grain sizes of the FeS_2 thin films annealed at 250 °C and 350 °C did not change, compared to that of the as-deposited thin films. The grain size of FeS_2 increased remarkably after being annealed at 450 °C, which is consistent with the grain size calculated from XRD peaks. In the intermediate temperature range of 250-450 °C, sulfur diffusion into the FeS_2 lattice can occur slowly, allowing the rearrangement of FeS_2 NCs. The grains tend to agglomerate and grow to a large scale. This explains the increasing grain size with increase of sulfurization temperature. Besides that, cracks and voids were observed on the surface of the FeS_2 thin films. In the intermediate temperature range of 250-450 °C, the surfactant of FeS_2 NCs will be decomposed partly, forming a very small blank between the FeS_2 NCs. The decomposition of surfactant decreases the surface area. The decreasing in surface area directly affects the microstructure of thin films [17,18]. By further increasing the sulfurization temperature, thermal roughening emerges. Additionally, grain size increasing is strengthened. These may explain the formation of cracks and voids.

The sulfurization temperature not only affects the grain size and crystallinity, but also the phase of FeS_2 films. The phase changes in the annealed iron pyrite thin films were characterized by Raman spectroscopy, which was found to be a substantially more sensitive technique than XRD in detecting the trace sulfide impurities in pyrite crystals. Fig. 3 shows the Raman spectra of the films on glass substrates at different sulfurization temperatures. Before annealing, the as-deposited films consisted of a pure pyrite phase. In Raman spectroscopy, for the pyrite peaks, two dominant bands

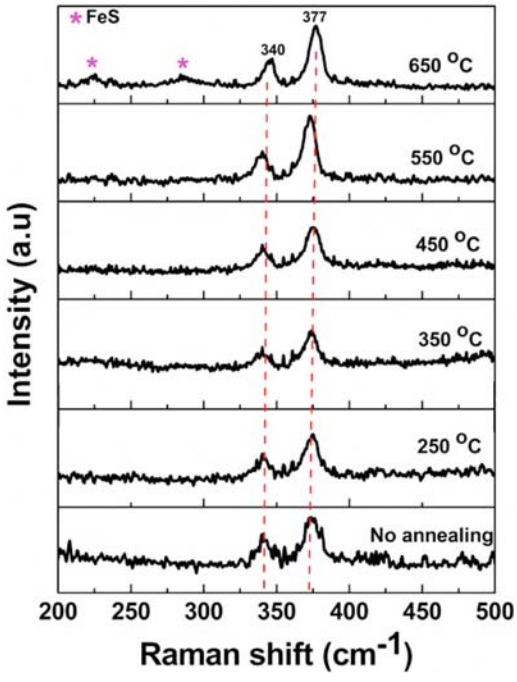

Fig. 3. Raman spectroscopy of FeS_2 thin films sulfurized at different temperatures.

were observed at 340 and 377 cm^{-1}, and a minor band at 429 cm^{-1}, corresponding to the Ag (S2 dumbbell vibration), Eg (S2 dumbbell stretching), and Tg (3) (vibration mode), respectively [11]. No peak for impurity phases was observed, which was confirmed by no peaks at 319-325 cm^{-1} for marcasite and 210-280 cm^{-1} for pyrrhotite (FeS phase). With increasing sulfurization temperature from 250 °C to 550 °C, the pyrite phase in the thin films did not change. On the other hand, at 650 °C sulfurization, the FeS phase emerged. At high temperature, the rate of FeS_2 decomposition to form FeS is higher than the S compensation from S-annealing to change FeS into FeS_2 phase. That explains why the FeS phase exits at high sulfurization temperature [19].

The elemental composition on the surface of FeS_2 thin films was studied by XPS (as shown in Fig. 4). XPS of FeS_2 films showed that the Fe 2p spectrum of pyrite has two major peaks at 707 eV (assigned as Fe 2p3/2) and 720 eV (assigned as Fe 2p1/2), which

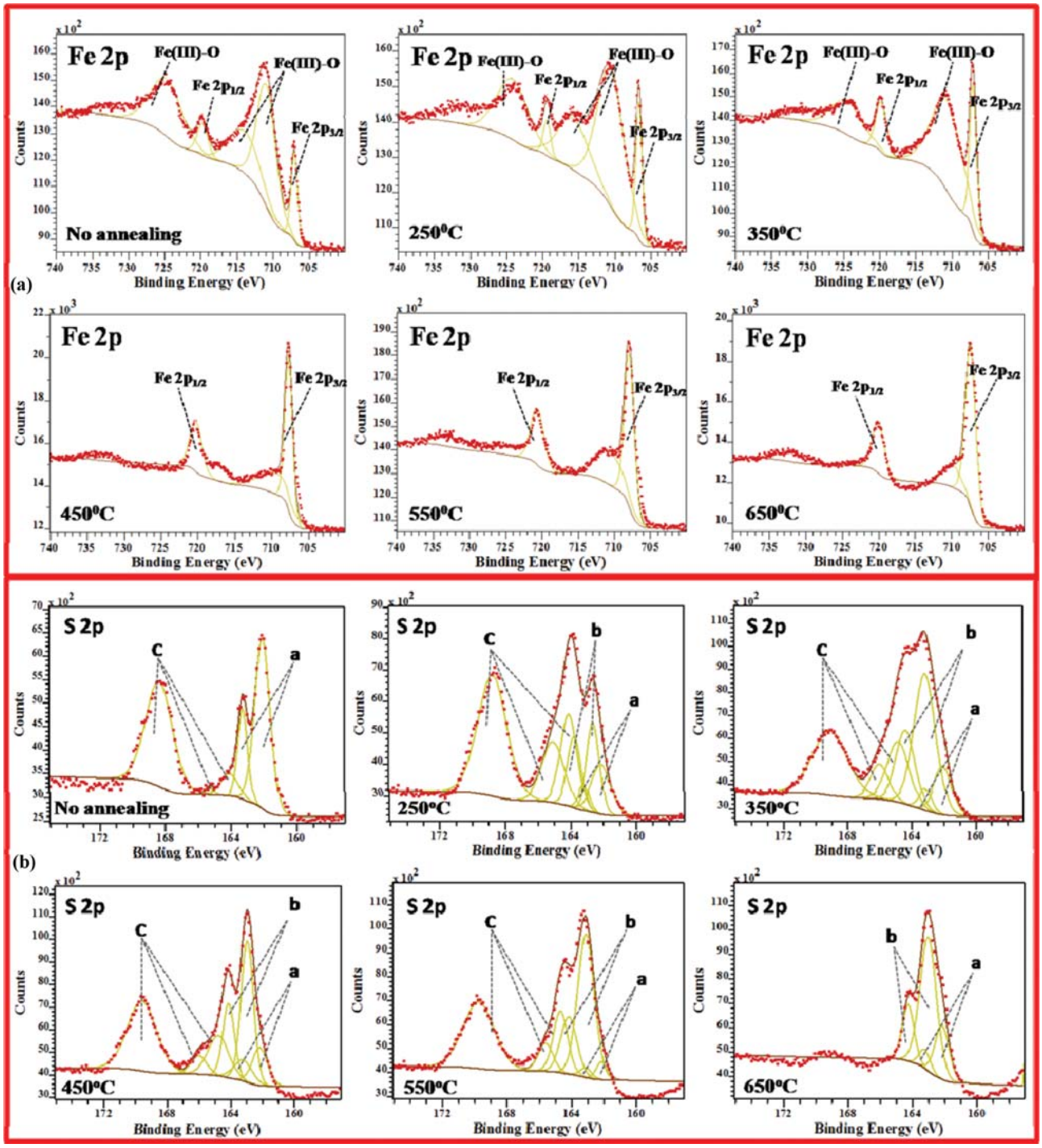

Fig. 4. XPS of (a) Fe 2p and (b) S 2p of FeS_2 thin films sulfurized at different temperatures.

illustrates the Fe^{2+} bulk peak (as shown in Fig. 4(a)). The peaks at the position of 711, 715, and 725 eV indicate the formation of Fe^{3+}-O surface states, which are formed by oxidation in air [20]. With increase of sulfurizing temperature in the range of 250 to 350 °C, the signal of the Fe bulk also increased. At the same time, the signal of Fe-O decreased. At 450 °C, the signal of Fe-O almost disappeared, while the signal of the Fe bulk dominated. Therefore, the change in surface properties depends on the annealing temperature. An increase in sulfurization temperature results in an increase in the grain size of FeS_2 NCs. When the grain size was increased, the surface area to bulk area ratios was also decreased [21]. This means that the oxidation of Fe^{2+} to Fe^{3+} on the surface of thin films also decreases. The sulfurization of FeS_2 thin films at an appropriate temperature would decrease the surface activity or increase the stability of the films to air oxidation.

Fig. 4(b) shows the S 2p spectrum of the surface thin films at different temperatures. The S 2p region was constructed in the couple peak of S 2p3/2 and S 2p1/2, in which the intensity ratio of S 2p3/2 and S 2p1/2 is 2 : 1. The interval energy of S $2p_{3/2}$ and S $2p_{1/2}$ is normally 1.1-1.2 eV [22]. Based on the peak fit of the S 2p spectrum, there are three main contributions to the S 2p region. The first contribution to the S 2p region is the peaks at 162.1 eV (S $2p_{3/2}$a) and 163.3 eV (S $2p_{1/2}$a), which represent the surface-most S atoms of the sulfur dimer located at the fracture surface (noted as S $2p_a$). The second contribution, centered at 162.8 eV and 164.0 eV, was assigned to the S $2p_{3/2}$b and S $2p_{1/2}$b (noted as S $2p_b$), respectively, which is the bulk core level of S bound as a disulfide group in iron pyrite. Each S atom is bonded to another S atom and three Fe^{2+} to produce S-S dimers with each atom being tetrahedrally coordinated. The third contribution is the large intensity in the region, 165-170 eV, where S-O moieties were observed (noted as S $2p_c$) [23]. The sulfurization at different temperatures affects the contribution of the S atom types to the S 2p region, which is illustrated by changing the intensity of the peak of the S atom type. Two kinds of S atoms exist on the surface of the non-annealed films. The first is the contribution of the sulfur surface, in which most S atoms are dominated because of the remarkable signal of the S $2p_a$ peaks. In addition, the intensity of S-O bonding can be observed in the region, 165-170 eV. In the range of 250 to 550 °C, the signal for the S $2p_a$ peaks decreased, while the signal for S $2p_b$ increased, and the signal of S $2p_c$ did not change significantly. At 650 °C, the signal for S $2p_c$ disappeared, while the signal for S $2p_b$ dominated. The S $2p_c$ signal disappeared due to the decomposition of the S-O component salt at temperatures higher 600 °C [24]. The domination of S $2p_b$ means that the higher the sulfurization temperature, the more the contribution of S atoms of the S-S dimer residing on the bulk site of pyrite.

2. Optical Properties

Fig. 5 shows the absorption spectra of the FeS_2 thin films as a function of the annealing temperature (Ts). In Fig. 5(a), all absorption curves tend to slope more and move to a higher photon energy upon increasing Ts and the tails, which are present as a low photon energy (0.5-0.9 eV), tend to disappear in the sulfurization process from 250 °C to 450 °C. On the other hand, at higher Ts, the absorption decreases slightly. The reason is that upon increasing sulfurization temperature to 450 °C, the sulfur vacancy densities

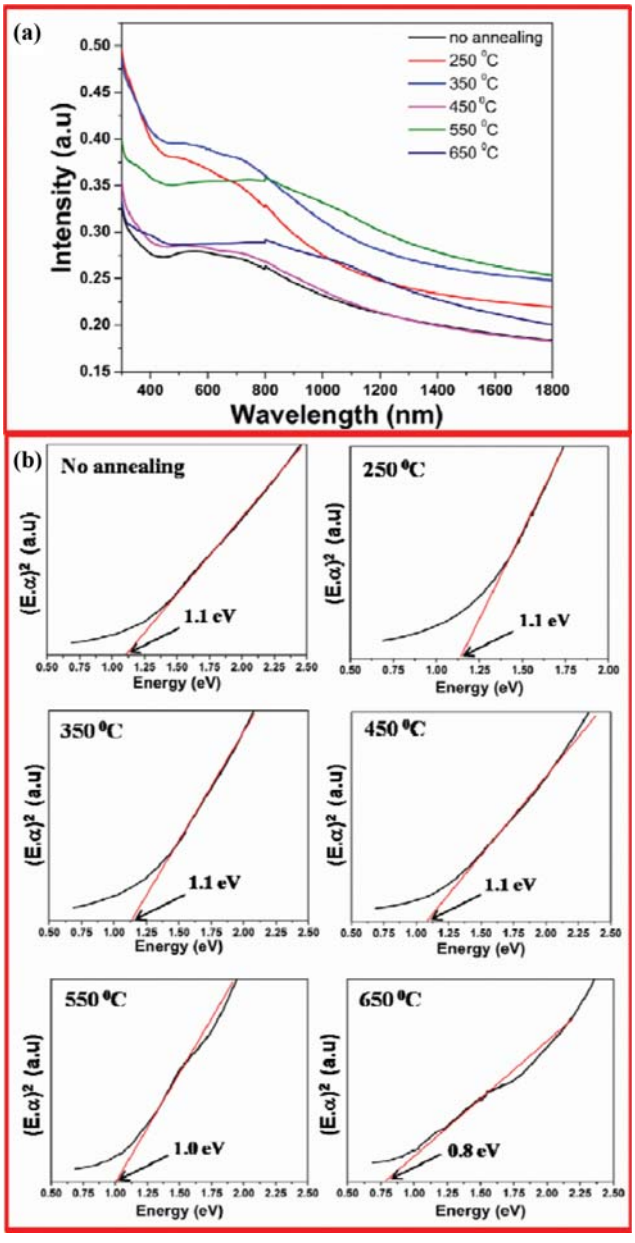

Fig. 5. (a) Absorption spectra and (b) plots of $(\alpha h\nu)^2$ vs. $h\nu$ of FeS_2 thin films sulfurized at different temperatures.

should decrease due to sulfur diffusion into the films. Moreover, the iron vacancy densities should also decrease due to the displacement of iron interstitials into their lattice natural position. This process should lead to a decrease in the optical absorption of the film at low photon energy and to a displacement of their absorption edge toward the higher photo energy, as observed by Sanches et al. [25]. In addition, increasing grain size or the reduction in the grain boundary density and the presence of voids and cracks might be responsible for the reduction in absorbance with increase of sulfurization temperature [26].

Fig. 5(b) shows the band gap (Eg) of the FeS_2 thin films, which can be obtained from an extrapolation of the straight-line portion of the $(\alpha h\nu)^n$ vs. hn plot to the horizontal ordinate axis. With n=2,

which is expected for a direct allowed transition, the best straight line was obtained for all films. The band gaps of the FeS_2 thin films changed slightly in the range of 0.8-1.2 eV, which is consistent with the reported value of a pyrite direct transition [11]. When the annealing was increased from 250-450 °C, the band gap was stable approximately at 1.1 eV. The band gap decreased noticeably to approximately 1.0 eV at 550 °C and 0.8 eV at 650 °C, which became an indirect transition. This means that the optical gap is almost constant up to a sulfurization temperature of ~450 °C and then decreases at higher temperatures, which is consistent with the results reported by Lifante group [27]. Normally, the decrease in band gap is the result of quantum confinement, which is deduced by the increasing the NPs size. In this research, however, there was no quantum confinement in FeS_2 NCs, because the size of the as-synthesized FeS_2 is not small enough to reach the Bohr diameter [28]. Therefore, quantum confinement resulting from an increase in size does not account for the decreasing band gap, even though the size of the FeS_2 increases with increasing Ts. The emergence of a FeS impurity phase (confirmed by Raman spectroscopy), which has a small band gap decreases the band gap of FeS_2 at 650 °C has been suggested. Potential fluctuations from the defect perturb the electronic band edges and can result in a broadening of the electronic states, leading to band tails extending below the band edges. This could manifest as sub-band gap optical absorption, which was confirmed by changing the shape of the absorption curve at the 1.5 eV energy level [29]. There has been some debate about identifying the band gap of FeS_2 NCs. Indeed, the reported optical properties of FeS_2 showed discrepancies, which suggest that the method used to obtain the Eg might not be the correct one in the case of pyrite [30]. In addition, the optical properties of FeS_2 thin films are difficult to study, because they depend on many factors, such as thickness, the morphology, and impurity phase.

3. The Electrical Properties

Electrical properties of the FeS_2 thin films were investigated using the Hall effect measurements. Fig. 6 shows the carrier concentration, electrical resistivity, and Hall mobility of the FeS_2 thin films annealed at different sulfurization temperatures. The FeS_2 thin films show the nature of the p-type semiconductor. In general, there are some intrinsic point defects in pyrite films, such as Fe vacancies, S vacancies, interstitial Fe atoms, and interstitial S atoms. The nature and number of defect types may decide the nature of the FeS_2 thin films, i.e., n-type or p-type. The Fe vacancies and interstitial S atoms act as acceptors to generate p-type carriers. On the other hand, the interstitial Fe atoms and S vacancies act as a donor to form n-type carriers. In the present case, a high temperature may increase the diffusion of sulfur vapor into the FeS_2 lattice [31]. This can decrease the S-vacancy defect and form the interstitial S atoms in the FeS_2 lattice, which decide the nature of p-type of FeS_2 thin films. The carrier concentration of the thin films changed unpredictably from 1.73×10^{17} to 6.29×10^{18} cm^{-3}. The change in carrier concentration cannot be explained, because it depends on the change in Hall mobility and resistivity of the thin films. The Hall mobility of the films tended to decrease from 2.78 to 0.1 $cm^2/V\cdot s$ when the sulfurization temperature was increased. The decrease in Hall mobility can be explained by two reasons: The first is reducing the impurity phases which played as the doping reagents in the FeS_2 lattice. The second is the formation of S-interstitial into the number of point defects on the surface of the thin film by sulfur diffusion into the lattice of FeS_2 at high temperatures, which was confirmed by changing the type of S-S in the surface of FeS_2 thin films in XPS S2p spectra [28]. This process may increase the point defects. Reducing the doping reagents and increasing the point defects may reduce the mobility of the thin films.

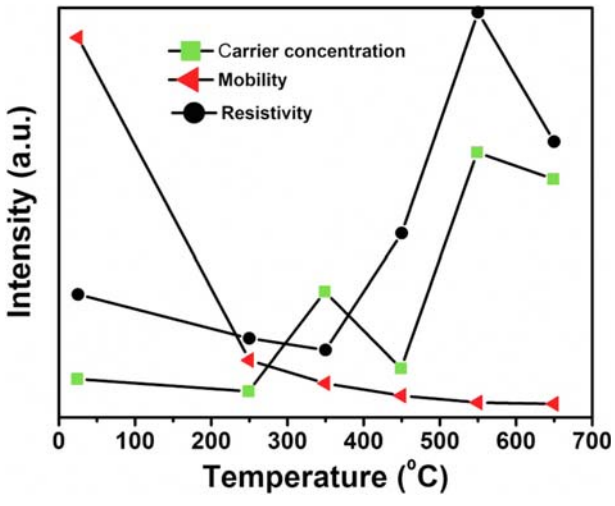

Fig. 6. Electrical resistivity, Hall mobility, and carrier concentration of FeS_2 thin films sulfurized at different temperatures.

The resistivity of FeS_2 thin films first decreases lightly from 35 to 0.85 Ω·cm with increasing sulfurization temperature to 350 °C. After that, the resistivity increases from 72 to 207 Ω·cm when sulfurization temperature increases from 450 to 650 °C. In a polycrystalline semiconductor, increasing the grain size or decreasing the grain boundary as well as increasing the crystallinity can reduce the resistivity of the thin films [32]. As observed by SEM, the films increased in size and crystalline with increasing the sulfurization temperature. Therefore, higher sulfurization temperatures should have decreased the resistivity of the thin films. In addition, polysulfide was detected by XPS, in which its concentration increased with increasing temperature, being the sulfur part diffused along the grain boundaries that also reduced the segregation of sulfur molecules in the boundaries. Reducing the segregation of sulfur molecules in the boundaries will decrease the resistivity of the films. In this study, the reducing resistivity tended to occur as described above at low sulfurization temperatures. On the other hand, the morphology of the surface thin films shows many cracks and voids, particularly in high-temperature sulfurization (at a temperature higher than 350 °C). The cracks and voids formed discontinuities and decreased the cross section area to electric conduction, which is the main reason for the increase in resistivity at temperatures higher 350 °C. That explains the decreasing of the resistivity of the thin films at a sulfurization temperature lower than 350 °C, while higher than 350 °C, the resistivity of the thin films increased strongly.

CONCLUSIONS

We examined the effects of sulfurization temperature on the

morphology, structure, and the optical and electrical properties of the FeS_2 thin films fabricated by spin coating from a suspension of 40 nm FeS_2 NCs. A change in the morphology and structure can facilitate a change in the optical and electrical properties. The increasing grain size and thermal strain facilitate cracks and voids on the surface of the thin films with increasing Ts. In particular, in high Ts (650 °C), the lower rate of S diffusion than S evaporation forms an impurity phase of FeS. The presence of a FeS phase with a low band gap is the main reason for the decreasing band gap of FeS_2 thin films in high Ts. A defect of the structure (impurity phase) and the surface (voids and cracks) can reduce the absorption. From 250-650 °C of the sulfurization process reducing the doping reagents and increasing the point defects may reduce the Hall mobility of the thin films. The resistivity of the FeS_2 thin films increased at high temperatures because of the emergence of many voids and cracks on the surface of the thin films. Based on the obtained results, the FeS_2 thin films should be sulfurized in the regime of temperature lower 550 °C to achieve the desirable properties of FeS_2 thin films for photovoltaic applications.

ACKNOWLEDGEMENTS

This work was supported by the Korea Institute of Energy Technology Evaluation and Planning (KETEP) and Ministry of Trade, Industry and Energy (MOTIE) of the Republic of Korea (grant no. 20163010012310).

REFERENCES

1. C. Wadia, A. P. Alivisatos and A. M. Kammen, *Environ. Sci. Technol.*, **43**, 2072 (2009).
2. F. Alharbi, J. D. Bass, A. Salhi, A. Alyamani, H. Kim and R. D. Miller, *Renewable Energy*, **36**, 2753 (2011).
3. Y. Bi, C. L. Exstrom, S. A. Darveau and I. Huang, *Nano Lett.*, **11**, 4953 (2012).
4. C. Steinhagen, T. B. Hatvey, C. J. Stolle, J. Harris and B. A. Korgel, *J. Phys. Chem. Lett.*, **3**, 2352 (2012).
5. L. Yu, S. Lany, R. Kykyneshi, V. Jieratum, R. Ravichandran, B. Pelatt, E. Altschul, H. A. S. Platt, J. F. Wage, D. A. Kesler and A. Zunger. *Adv. Energy Mater.*, **1**, 748 (2011).
6. T. Nakada, H. Ohbo, T. Watababe, H. Nakazawa, M. Matsui and A. Kunioka, *Sol. Ener. Mater and Sol. Cells*, **49**, 285 (1997).
7. C. Sanchez, C. Heras and I. J. Ferrer, *SPIE*, **1729**, 172 (1990).
8. A. Yamamoto, N. Makamura, A. Seki, E. L. Li, A. Hashimoto and S. Nakamura, *Sol. Energy Matt. Sol. Cells*, **75**, 451 (2003).
9. Y. Dong, Y. Yeng, H. Duan, Y. Sun and Y. Chen, *Matt. Lett.*, **59**, 2398 (2005).
10. V. Aluri, K. T. R Reddy and Y. M. Reddy. *Nanotechnol. Rev.*, **4**, 469 (2015).
11. C. Delas Heras and G. Lifante, *J. Appl. Phys.*, **82**, 5132 (1997).
12. S. Seefeld, M. Limpinsel, Y. Liu, A. Weber, Y. Zhang, N. Berry, Y. J. Kwon, C. L. Perkins, J. C. Hemmiger, R. Wu and M. Law, *J. Am. Chem. Soc.*, **135**, 4412 (2013).
13. J. Puthussery, S. Seefeld, N. Berry, M. Gibbs and M. Law, *J. Am. Chem. Soc.*, **133**, 716 (2011).
14. Z. Shi, A. H. Jayatissa and F. C. Peiris, *J. Mater. Sci.: Mater. Electron.*, **27**, 535 (2015).
15. S. Hsiao, K. Wu, S. Huang, S. Liu, S. Chiu and L. Chou, *The Jan. Soc. Appl. Phys.*, **8**, 201 (2015).
16. B. Holger, V. S. Elena, A. Robert, I. Mekis, A. Kornowski, G. Grubel and H. Weller, *Langmuir*, **21**, 1931 (2005).
17. B. Mao, Q. Dong, C. L. Exstrom and J. Huang, *Thin Solid Film*, **562**, 361 (2014).
18. F. Wang, L. Huang, Z. Luan, J. Huang and L. Meng, *Mater. Chem. Phys.*, **132**, 505 (2012).
19. R. J. Soukup, P. Prabukantha, N. J. Lanno, A. Sarkar, C. A. Kamler, et al., *J. Vac. Sci. Technol. A*, **29**, 11001 (2011).
20. H. W. Mesbitt, M. Saini, H. Hochst, G. M. Bancroft, A. G. Schaufuss and R. Szargan, *American Mineralogist*, **85**, 850 (2000).
21. I. E. Dubois, S. Holgersson and S. Allard, *Water- rock interaction*, Taylor & Francis Publication, London, 717 (2010).
22. R. Murphy and D. R. Strongin, Surface Science Reports, **64**, 1 (2009).
23. S. Chaturvedi, R. Katz, J. Guevremont, M. A. Choon and D. R. Strong, *American Mineralogist*, **81**, 261 (1996).
24. M. Huska, M. Koskenlinna and L. Ninisto, *J. Appl. Chem. Biotechnol.*, **26**, 129 (1916).
25. C. Delas Heras, I. J. Ferrer, D. M. Nevskaia and C. Sanches, *J. Appl. Phys.*, **74**, 4551 (1993).
26. F. wang, L. Huang, Z. Luan, J. Huang and L. Meng, *Mater. Chem. Phys.*, **132**, 505 (2012).
27. C. D. Geras and G. Lifante, *J. Appl. Phys.*, **82**, 5132 (1997).
28. W. Li, M. Dolinger, A. Vaneski, A. L. Rogach, F. Jackel and J. Feldmann, *J. Mater. Chem.*, **21**, 17946 (2011).
29. S. Shukla, G. Xing, H. Ge, R. R. Prabhakar, S. Mathew, Z. Su, V. Nalla, T. Venkatesan, N. Mathews, T. Sritharan, T. C. Sum and Q. Xiong, *ACS Nano*, **10**, 4431 (2016).
30. I. J. Ferrer, D. M. Nevskaia, C. Delas Heras and C. Sanches, *Solid State Communications*, **74**, 913 (1990).
31. D. F. Pridmore and R. T. Shuey, *American Mineralogist*, **61**, 248 (1976).
32. L. Huang, Y. Liu and L. Meng, *J. Mater. Sci. Technol.*, **25**, 237 (2009).